Analytical Study of Current Distribution in a 2-Turn Non-Insulated HTS Coil

Marco Breschi, *Senior Member, IEEE*, Massimo Fabbri, Antonio Macchiagodena, and Luca Bottura

***Abstract*—High-Temperature Superconducting (HTS) coils have gained increasing attention in various applications, such as magnetic energy storage systems, fusion reactors, and high field magnets, due to their superior current-carrying capability and reduced power loss. One of the challenges in the design of these coils is the distribution of current between the individual turns, particularly for non-insulated or metal-insulated HTS coils. This work presents an analytical solution for determining the current distribution between the turns of a 2-turn non-insulated HTS coil. The proposed model enables the assessment of the local currents in steady state conditions. The solution is validated through numerical simulations performed with a non-linear electric circuit model. The results show the impact on current distribution of the main coil parameters, such as the coil radius, the turn-to-turn contact conductance and the resistance of joints or defects between turns.**

***Index Terms*—Fusion magnets, high field magnets, non-insulated coils, partially insulated coils, HTS coils, current distribution.**

I. Introduction

THE non-insulated High-Temperature Superconducting (NI-HTS) coils, which lack of conventional insulation between turns, have attracted significant attention for their applications in superconducting high-field magnets and other research areas [1], [2], [3], [4], [5], [6]. A key aspect of the behavior of the NI-HTS coil is the current distribution between turns, which directly affects the electromagnetic response and stability of the coil [7], [8], [9]. Accurate modeling of the current distribution is crucial for guiding the design of NI-HTS coils and magnets, enabling controlled current sharing and reliable operation. While a range of numerical models with different accuracy and complexity have been proposed to study NI-HTS coil electromagnetics [10], [11], [12], [13], [14], [15], [16], [17], no simplified analytical descriptions of the underlying physical processes have, to our knowledge, been presented.

This work presents an analytical framework for evaluating the steady-state current distribution in a two-turn NI-HTS coil. The model incorporates the effects of turn-to-turn contact, coil geometry, and the impact of localized joint resistance, providing a detailed description of the current distribution and of its dependence on the main model parameters. Validation is performed through numerical simulations using the nonlinear electric circuit model CALYPSO [16], [17]. This work is limited to the study of current distribution in 2-turn coils. In the past, models based on similar approaches were developed for the analysis of current distribution in 2-strand superconducting cables [18], [19], [20]. Later investigations extended the analysis to multistrand cables consisting of an arbitrary number of strands [21]. A similar evolution is envisioned for this research, with the aim to extend the model developed here for the 2-turn coils to windings consisting of an arbitrary number of turns. The 2-turn model presented here cannot be directly applied to the study of a coil consisting of many turns. However, it can be applied to study real cases in which the 2 turns involved are those before and after a localized permanent defect arising from construction issues or coil inhomogeneities. As a matter of fact, the steady state current distribution, even in a large coil, mainly takes place in the turns close to the defect. The current distribution patterns may differ from the case of *N*-turn coils, but the dimensionless quantities defining the problem are still the same.

Received 17 October 2025; revised 15 December 2025, 21 January 2026, and 20 February 2026; accepted 24 February 2026. Date of publication 3 March 2026; date of current version 18 March 2026. *(Corresponding author: Marco Breschi.)*

Marco Breschi, Massimo Fabbri, and Antonio Macchiagodena are with the Department of Electrical, Electronic and Information Engineering, Alma Mater Studiorum – Università di Bologna, 40136 Bologna, Italy (e-mail: marco.breschi@unibo.it).

Luca Bottura is with CERN, 1217 Geneva, Switzerland (e-mail: luca.bottura@cern.ch).

Color versions of one or more figures in this article are available at https://doi.org/10.1109/TASC.2026.3669565.

Digital Object Identifier 10.1109/TASC.2026.3669565

II. NI Coil Electrical Model

A. Model Assumptions

The present study of non-insulated coils is focused on the analysis of either a one-layer solenoid, with turns in contact along the length of solenoid, or a single pancake, with turns in contact in radial direction. In both cases, all turns are assumed to have the same length, and each turn is in resistive contact only with the previous and the following one. The mutual induction coupling is considered between all turns of the coil.

A sketch of the coil geometry and of its main parameters is shown in Fig. 1. The coil has radius a; the variable ϑ represents the angular coordinate along one turn ($0 \leq \vartheta \leq 2\pi$), while ϑ_c is the central angular coordinate, i.e., $\vartheta_c = \vartheta - \pi$. The coil is described through a distributed parameters model, shown in Fig. 2 for the simplified case of the 2-turn coil.

The operation current I_{op} (t) enters the first turn, eventually redistributes towards the second turn through the distributed contact conductance g and finally exits from the second turn. Each turn is characterized by a given resistance per unit length r, while a lumped resistance R is located between the two turns

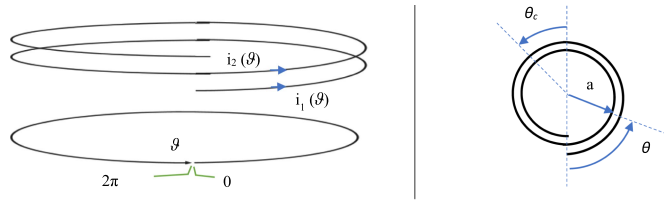

Fig. 1. Sketch of the NI coil and its main geometrical parameters. The angles θ and θ_c are set to zero at the beginning and at the center of each turn respectively.

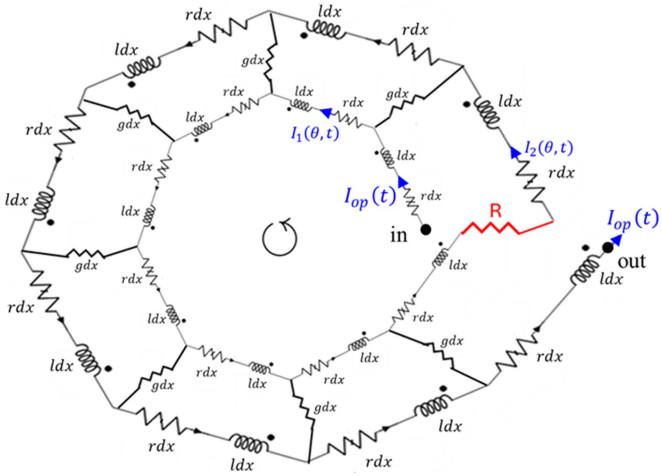

Fig. 2. Schematics of the linear, distributed parameters electrical circuit model adopted to describe the NI-coil with 2 turns through the analytical approach.

to represent either a joint, a local defect or a resistive zone corresponding to a quench.

The parameter *l* represents the per unit length self-inductance while *m* is the per unit length mutual inductance.

B. Model Equations

The main electrical variables of the distributed parameter electric circuit are the following: i_k (ϑ, t) is the current in turn *k* [A], v_k (ϑ, t) is the voltage between the beginning and a given position in turn *k* [V]. Currents and voltages can be grouped in the current and voltage vectors, denoted as $\boldsymbol{i}$(ϑ, t) and $\boldsymbol{v}$(ϑ, t) respectively. The circuit equations can be written as follows:

$$\frac{\partial \boldsymbol{v}}{\partial (a\vartheta)}(\vartheta,t) = -r\boldsymbol{i}(\vartheta,t) - \int_0^{2\pi} \boldsymbol{m}(\vartheta,\vartheta') \cdot \frac{\partial \boldsymbol{i}}{\partial t}(\vartheta',t)\, d(a\vartheta') \tag{1}$$

$$\frac{\partial \boldsymbol{i}}{\partial (a\vartheta)}(\vartheta,t) = \boldsymbol{g}\cdot\boldsymbol{v}(\vartheta,t) \tag{2}$$

where:

$$\boldsymbol{g} = \begin{bmatrix} -g & g \\ g & -g \end{bmatrix}$$

$$\boldsymbol{m}(\vartheta,\vartheta') = \begin{bmatrix} l(\vartheta,\vartheta') & m(\vartheta,\vartheta') \\ m(\vartheta,\vartheta') & l(\vartheta,\vartheta') \end{bmatrix} \tag{3}$$

The expressions of l and m are given by:

$$l(\vartheta,\vartheta') = \frac{\mu_0}{4\pi}\frac{\cos(\vartheta-\vartheta')}{\sqrt{\varepsilon^2+2a^2-2a^2\cos(\vartheta-\vartheta')}} \tag{4a}$$

$$m(\vartheta,\vartheta') = \frac{\mu_0}{4\pi}\frac{\cos(\vartheta-\vartheta')}{\sqrt{h^2+2a^2-2a^2\cos(\vartheta-\vartheta')}} \tag{4b}$$

where ε and h are infinitely small quantities added to avoid divergence in the expressions. The following boundary and initial conditions were considered for the study:

$$i_1(\vartheta=0,t) = I_{op}(t);\ i_2(\vartheta=0,t) = i_1(\vartheta=2\pi,t)$$

$$v_1(\vartheta=0,t) = 0; \tag{5a}$$

$$v_2(\vartheta=0,t) = v_1(\vartheta=2\pi,t) - R\,i_1(\vartheta=2\pi,t) \tag{5b}$$

$$i_1(\vartheta,t=0) = i_{1,0}(\vartheta);\ i_2(\vartheta,t=0) = i_{2,0}(\vartheta)$$

$$v_1(\vartheta,t=0) = v_2(\vartheta,t=0) = 0 \tag{6}$$

We define $V_{op}(t)$ the unknown operational voltage as $V_{op}(t) = v_2(\vartheta = 2\pi, t)$. Given the peculiar symmetry of the system, the following equations also hold:

$$i_1(2\pi-\vartheta,t) = i_2(\vartheta,t)$$

$$i_2(2\pi-\vartheta,t) = i_1(\vartheta,t) \tag{7a}$$

$$v_1(2\pi-\vartheta,t) = V_{op}(t) - v_2(\vartheta,t)$$

$$v_2(2\pi-\vartheta,t) = V_{op}(t) - v_1(\vartheta,t) \tag{7b}$$

C. Model Solution

To simplify the notation, time dependence is omitted hereafter, while it is still implicitly assumed. Equations and boundary conditions can be decoupled, noting that both inductance and conductance matrices are linearly related to the same nondimensional matrix [A]:

$$[A] = \begin{bmatrix} 1 & -1 \\ -1 & 1 \end{bmatrix};\ \boldsymbol{g} = -g[A];\ \boldsymbol{m} = (l+m)[1] - m[A] \tag{8}$$

The eigenvalues and normalized eigenvectors of matrix [A] are given by $\lambda_1 = 0$, $\lambda_2 = 2$, and $u_1 = [1/\sqrt{2} \quad 1/\sqrt{2}]^T$, $u_2 = [-1/\sqrt{2} \quad 1/\sqrt{2}]^T$. Defining the orthogonal matrix [q] = [u_1, u_2], and decomposing the matrix [A] = [q][Λ][q]^T, where [Λ] = diag(0,2), both inductance and conductance matrices are diagonalized with the same eigenvectors. After defining $l_s = l+m$, $l_d = l-m$ the expression of $\boldsymbol{g}$ and $\boldsymbol{m}$ are:

$$\boldsymbol{g} = -g[q][\Lambda][q]^T;\ \boldsymbol{m} = [q]\ diag(l_s,l_d)[q]^T \tag{9}$$

The corresponding normal modes are defined as:

$$i_1'(\vartheta) = \frac{i_1(\vartheta)+i_2(\vartheta)}{\sqrt{2}};\ i_2'(\vartheta) = \frac{-i_1(\vartheta)+i_2(\vartheta)}{\sqrt{2}} \tag{10a}$$

$$v_1'(\vartheta) = \frac{v_1(\vartheta)+v_2(\vartheta)}{\sqrt{2}};\ v_2'(\vartheta) = \frac{-v_1(\vartheta,t)+v_2(\vartheta)}{\sqrt{2}} \tag{10b}$$

It is worth noting that the normal modes correspond to the sum and difference of currents and voltages. To simplify the notation,

the normal modes are referred hereinafter as $i_s = i_1\,'(\vartheta)$ and $i_d = i_2{}'(\vartheta)$ where *s* and *d* stand for (scaled) sum and difference; a similar notation is used for the voltages. The equations can thus be rewritten in terms of normal modes:

$$\frac{\partial v_s}{\partial\,(a\vartheta)}\;(\vartheta) = -r i_s\,(\vartheta) - \int_0^{2\pi} l_s\,(\vartheta,\vartheta')\,\frac{\partial i_s}{\partial t}\,(\vartheta')\;d\,(a\vartheta') \tag{11a}$$

$$\frac{\partial i_s}{\partial\,(a\vartheta)}\;(\vartheta) = 0 \tag{11b}$$

$$\frac{\partial v_d}{\partial\,(a\vartheta)}\;(\vartheta) = -r i_d\,(\vartheta) - \int_0^{2\pi} l_d\,(\vartheta,\vartheta')\,\frac{\partial i_d}{\partial t}\,(\vartheta')\;d\,(a\vartheta') \tag{11c}$$

$$\frac{\partial i_d}{\partial\,(a\vartheta)}\;(\vartheta) = -2g v_d\,(\vartheta) \tag{11d}$$

D. Steady State Solution

The general solution of (11) in transient conditions is complex and is beyond the scope of this work. The stationary solution of (11) is the asymptotic limit of the general time dependent solution. Details on the derivation of the steady state solution are reported in the Appendix.

The problem solution exhibits two main dependencies: the current redistribution length, given by $1/\sqrt{2gr}$, and the ratio between the lumped resistance *R* and the total resistance of one turn, given by $2\pi ar$. It is therefore useful to define two nondimensional parameters $A = a\sqrt{2gr}$ and $\chi = R/2\pi ar$.

The steady state solution can be expressed as the ratio of the total coil voltage $V_{op,\,DC}$ to the operation current $I_{op,DC}$, both in DC conditions:

$$-\frac{V_{op,\,DC}}{I_{op,\,DC}} = 2\pi ar\,\frac{\chi\pi A\sinh(\pi A) + (2+\chi)\cosh(\pi A)}{\cosh(\pi A) + (2\chi+1)\,\pi A\sinh(\pi A)} \tag{12}$$

For *g* small enough, $A<<1$: $-\frac{V_{op,\,DC}}{I_{op,DC}} \approx 4\pi ar + R$. In this condition, the currents do not redistribute from turn to turn, but flow along the turns and on the joint resistance *R,* as is the case in an insulated coil.

For *R* small enough, $\chi \approx 0$ the solution is $-\frac{V_{op,DC}}{I_{op},DC} \approx \frac{4\pi ar}{1+\pi A\tanh(\pi A)}$, which tends to $4\pi ar$ for very small *g* (insulated coil). In the perfectly superconducting state, with $r \to 0^+$ and non-zero *R,*(12) becomes $-\frac{V_{op,DC}}{I_{op,DC}} = \frac{1}{2\pi ag+\frac{1}{R}}$ which represents the parallel connection between *R* and the conductance $2\pi ag$.

III. Results and Discussion

A. Numerical Model

To keep CALYPSO consistent with the assumptions of the analytical one, the superconducting tape composing the two-turn coil is subdivided in only two electrical elements across its width, thus ensuring a uniform current distribution in this direction. Another simplification concerns the definition of the longitudinal resistances of the turns. These resistances are not modeled with the power law but rather set to a constant value R_l.

TABLE I
Simulation Parameter

N_d	100	r	3 10^{-8} Ω/m
a	0.1–1 m	g	2 10^{7} S/m
$I_{op,MAX}$	200 A	t_r	4 s

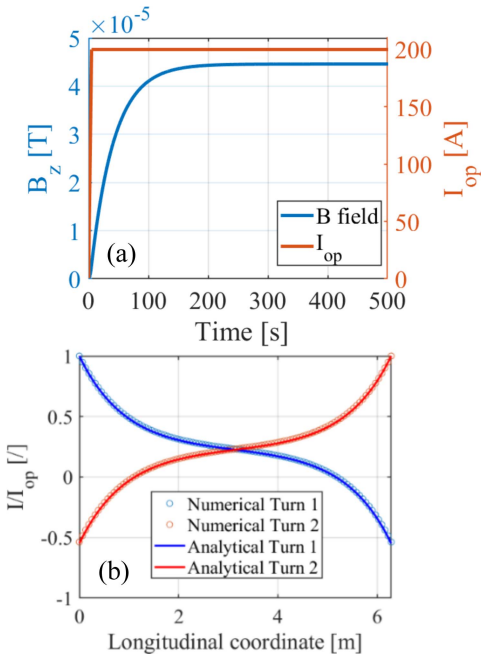

Fig. 3. (a) Comparison between the longitudinal currents computed with the analytical formulation and by CALYPSO for a 1 m radius coil. (b) Operating current and axial magnetic field at the coil barycenter computed with CALYPSO.

The contact *resistances* between the two turns in radial direction are all set to a constant value R_{con}. The definitions of both R_l and R_{con} are given as follows:

$$R_l = 4\pi ar/N_d;\;\; R_{con} = (N_d - 1)/\pi ag \tag{13}$$

where N_d is the number of elements in which each individual turn is discretized.

B. Benchmark of the Analytical Formulae

The analytical formulae presented here were compared with the results of CALYPSO in several case studies, which also allows one assessing the impact of the key parameters *a*, *g*, *r* and *R* (not considered in these test cases). The parameters used in these simulations are listed in Table I. The simulations performed aim at highlighting the impact of the coil radius. In the simulations the current rises with a constant ramp rate from 0 to $I_{op,\,MAX}$ in a time t_r and then stays constant at the peak value during a flat-top period.

The results in terms of current distribution along the turns of the coil are presented in Figs. 3 and 4. Fig. 3(a) shows the time evolution of the operating current and of the axial component of the magnetic field at the barycenter of the coil computed with CALYPSO. It is worth noting that the axial magnetic field component, which directly depends on the azimuthal component

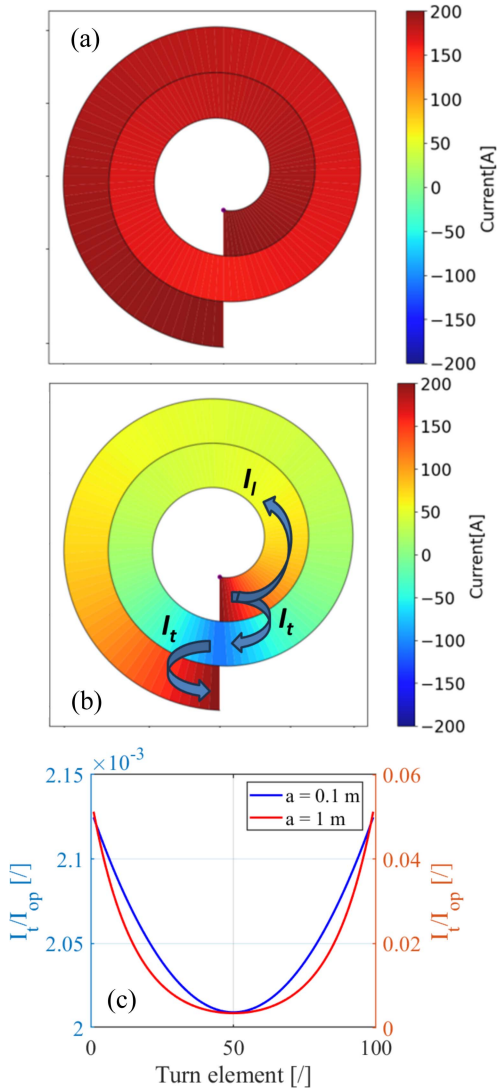

Fig. 4. 2D current distribution map, not in scale, computed with (A7) along the 2-turns of an NI-coil with (a) coil radius $a = 0.1$ m and (b) coil radius $a = 1$ m. I_l indicates the longitudinal current and I_t the transverse one. (c) Transverse current distribution along the turn (taken positive from turn #1 to turn #2).

of the current, reaches its steady state more than 300 s after the start of the current flat-top. The asymptotic limit of this transient represents the DC solution to be compared with the analytical formulae.

Fig. 3(b) shows the excellent agreement between the results of the DC current distribution along the two turns computed with the analytical formulae (see A7) and the CALYPSO code. Notably, the current in the first turn decreases along the turn and even changes sign; a symmetric behavior is observed in the second turn.

In Fig. 4(a), corresponding to a coil radius set to 0.1 m, the current distribution exhibits no flow inversion: the longitudinal current is slightly reduced with a minimum in the region of connection of the two turns. In contrast, Fig. 4(b), corresponding to the 1 m radius coil, shows that the longitudinal current exhibits a sign change. For the larger radius coil, the effect of the transverse conductance is more pronounced: the longitudinal current is equal to $I_{op,\,MAX}$ (see Table I) at the beginning of the first turn but then is reduced by the radial currents flowing towards the coil end. The sign change occurs near the terminal since the current path of least resistance does not follow the longitudinal direction from the input to the output terminal. A portion of the transport current is thus short-circuited by the contact conductance between the two turns.

The different behavior of the two coils can also be observed in Fig. 4(c), which shows a much higher transverse current flowing in the large coil with respect to the small one. It should be noted that the crucial parameter driving the current distribution is A. Different combinations of the values of a, g, r corresponding to the same value of A result in the same normalized current distribution at steady state.

IV. Conclusion

In this work, an analytical solution was developed to determine the current distribution between the turns of a 2-turn NI HTS coil. The proposed model provides a straightforward method to assess local currents under steady-state conditions. A benchmark against numerical simulations with an electric circuit model shows excellent agreement, confirming the reliability of this approach. The results highlight that the current distribution in NI-HTS coils is strongly influenced by key factors such as coil geometry, contact conductance between turns, and resistivity of the turns. The interplay between these parameters can lead to significant variations in the longitudinal and radial current distributions. Even in steady-state regime, the longitudinal transport current producing the desired axial magnetic field is lower than the operation current, as part of it is diverted into permanent radial currents, especially for high values of the defect resistance.

The model developed shows peculiar current distribution phenomena, such as the inversion of current in the vicinity of the coils ends, which could affect the coil performance. These effects, confirmed here by numerical analysis, should not depend on the number of turns and will be the subject of further investigations on N-turn coils. This analytical framework may constitute a tool for the benchmarking of numerical codes.

Appendix

Writing (11a) and (11b) in the central reference frame, and imposing stationary\ conditions, yields:

$$\frac{\partial}{\partial \vartheta_c} v_{cs}\ (\vartheta_c) = -ari_{cs}\,(\vartheta_c)\,;\ \frac{\partial}{\partial \vartheta_c} i_{cs}\ (\vartheta_c) = 0 \qquad \text{(A1)}$$

It can be noticed that i_{cs} does not depend on ϑ_c, and that the first term of(A1) can be integrated using (10) to obtain $v_s\,(\pi) = v_{cs}\,(0) = V_{op}\,/\sqrt{2}$:

$$v_{cs}\ (\vartheta_c) = -ari_{cs}\,\vartheta_c + \frac{V_{op,DC}}{\sqrt{2}};\ i_{cs}\ (\vartheta_c) = i_{cs} \qquad \text{(A2)}$$

Therefore, applying the definition of A and χ yields:

$$i_{cs} = \frac{I_{op,DC}}{(1+\chi)}\left(\chi - \frac{V_{op,DC}}{2\pi ar I_{op,DC}}\right)\frac{\sqrt{2}}{2} \qquad \text{(A3)}$$

Notice that i_{cs} remains undetermined until the operational voltage (or the DC characteristics) is found.

Writing (11c) and (11d) in the central reference frame yields:

$$\frac{\partial}{\partial \vartheta_c} v_{cd}\ (\vartheta_c) = -ar i_{cd}\,(\vartheta_c)\ \frac{\partial}{\partial \vartheta_c} i_{cd}\ (\vartheta_c) = -2ag v_{cd}\,(\vartheta_c) \tag{A4}$$

The two expressions in (A4) are in the same form

$$\frac{\partial^2}{\partial {\vartheta_c}^2} F\ (\vartheta_c) = A^2\ F\,(\vartheta_c)\ . \tag{A5}$$

Using parity, it is possible to choose the correct solution between $sinh(\vartheta_c A)$ and $cosh(\vartheta_c A)$, thus obtaining:

$$\begin{aligned} i_{cd}(\pi) &= -\left(\frac{V_{op,DC}}{2\pi ar} - \chi I_{op,DC}\right) \frac{\sqrt{2}}{2} \frac{\pi A \tanh(\pi A)}{1+\chi\pi A \tanh(\pi A)} \\ &\quad \times R i_{cd}(\pi) + (V_{op,DC} - R I_{op,DC})\ \frac{\sqrt{2}}{2} \\ &= \pi ar \left(\frac{V_{op,DC}}{2\pi ar} - \chi I_{op,DC}\right) \frac{\sqrt{2}}{1+\chi\pi A \tanh(\pi A)} \end{aligned} \tag{A6}$$

The DC solution for the current in the two turns can finally be expressed as a combination of the sum and difference currents as in (A7a) and (A7b). The same can be done for the voltages, which are omitted here.

$$\frac{i_1\,(\vartheta)}{I_{op,DC}} = \frac{\cosh(\pi A) + \chi\pi A \sinh(\pi A) + (1+\chi)\,\pi A \sinh(\pi - \vartheta)\,A}{\cosh(\pi A) + (2\chi+1)\,\pi A \sinh(\pi A)} \tag{A7a}$$

$$\frac{i_2\,(\vartheta)}{I_{op,DC}} = \frac{\cosh(\pi A) + \chi\pi A \sinh(\pi A) - (1+\chi)\,\pi A \sinh(\pi - \vartheta)\,A}{\cosh(\pi A) + (2\chi+1)\,\pi A \sinh(\pi A)} \tag{A7b}$$

REFERENCES

[1] S. Hahn, D. K. Park, J. Bascunan, and Y. Iwasa, "HTS pancake coils without turn-to-turn insulation," *IEEE Trans. Appl. Supercond.*, vol. 21, no. 3, pp. 1592–1595, Jun. 2011.

[2] J. Kosse et al., "Design of NI HTS solenoid for PSI positron production experiment," *Supercond. Sci. Technol.*, vol. 38, no. 3, 2025, Art. no. 035008.

[3] C. C. Chow, M. D. Ainslie, and K. Chau, "High temperature superconducting rotating electrical machines: An overview," *Energy Rep.*, vol. 9, pp. 1124–1156, 2023.

[4] J. Kim et al., "Investigation about the effects of metal-clad winding on the electromagnetic characteristics of the GdBCO racetrack coils in a time varying magnetic field," *Results Phys.*, vol. 11, pp. 400–405, 2018.

[5] G. Kim et al., "Investigation on nonuniform current density and shape deformation affecting the magnetic field performance of a saddle-shaped no-insulation HTS cosine–theta dipole magnet," *Supercond. Sci. Technol.*, vol. 36, no. 8, 2023, Art. no. 084002.

[6] Z. S. Hartwig et al., "The SPARC toroidal field model coil program," *IEEE Trans. Appl. Supercond.*, vol. 34, no. 2, Mar. 2024, Art. no. 0600316.

[7] S. Hahn et al., "No-insulation coil under time-varying condition: Magnetic coupling with external coil," *IEEE Trans. Appl. Supercond.*, vol. 23, no. 3, Jun. 2013, Art. no. 4601705.

[8] D. Liu, H. Yong, and Y. Zhou, "Analysis of charging and sudden discharging characteristics of no-insulation ReBCO coil using an electromagnetic coupling model," *AIP Adv.*, vol. 7, no. 11, 2017, Art. no. 115104.

[9] M. Cho et al., "Combined circuit model to simulate post-quench behaviors of No-insulation HTS coil," *IEEE Trans. Appl. Supercond.*, vol. 29, no. 5, 2019, Art. no. 4901605.

[10] S. Noguchi, R. Itoh, S. Hahn, and Y. Iwasa, "Numerical simulation of superconducting coil wound with no-insulation NbTi wire," *IEEE Trans. Appl. Supercond.*, vol. 24, no. 3, Jun. 2014, Art. no. 4900504.

[11] S. Noguchi and S. Hahn, "A newly developed screening current simulation method for rebco pancake coils based on extension of PEEC model," *Supercond. Sci. Technol.*, vol. 35, no. 4, 2022, Art. no. 044005.

[12] L. Qin et al., "Refined circuit model for current distribution of the no-insulation HTS insert magnet," *Supercond. Sci. Technol.*, vol. 34, no. 7, 2021, Art. no. 075002.

[13] R. Mataira, M. D. Ainslie, R. Badcock, and C. W. Bumby, "Modelling parallel-connected, No-insulation high-T_c superconducting magnets," *IEEE Trans. Appl. Supercond*, vol. 31, no. 5, Aug. 2021, Art. no. 4602205.

[14] X. Wang et al., "Turn-to-turn contact characteristics for an equivalent circuit model of no-insulation ReBCO pancake coil," *Supercond. Sci. Technol*, vol. 26, no. 3, 2013, Art. no. 035012.

[15] E. Pardo and P. Fazilleau, "Fast and accurate electromagnetic modeling of non-insulated and metal-insulated REBCO magnets," *Supercond. Sci. Technol*, vol. 37, no. 3, 2024, Art. no. 035016.

[16] M. Breschi, A. Macchiagodena, P. L. Ribani, A. Musso, G. Angeli, and M. Bocchi, "Circuit model of interlayer and screening currents in layer-wound NI HTS coils," *IEEE Trans. Appl. Supercond*, vol. 34, no. 3, May 2024, Art. no. 4604505.

[17] M. Breschi, A. Macchiagodena, P. L. Ribani, A. Musso, G. Angeli, and M. Bocchi, "Improvement of the circuit analyzer problem solver CALYPSO," *IEEE Trans. Appl. Supercond*, vol. 35, no. 5, Aug. 2025, Art. no. 4902305.

[18] G. Ries, "Stability in superconducting multistrand cables," *Cryogenics*, vol. 20, no. 9, pp. 513–519, 1980.

[19] L. Krempasky and C. Schmidt, "Theory of 'supercurrents' and their influence on field quality and stability of superconducting magnets," *J. Appl. Phys.*, vol. 78, no. 9, pp. 5800–5810, 1995.

[20] L. Krempasky and C. Schmidt, "Experimental verification of 'supercurrents' in superconducting cables exposed to AC-fields," *Cryogenics*, vol. 39, no. 1, 1999, pp. 23–33, doi: 10.1016/S0011-2275(99)00003-X.

[21] L. Bottura, M. Breschi, and M. Fabbri, "Analytical solution for the current distribution in multistrand superconducting cables," *J. Appl. Phys*, vol. 92, no. 12, pp. 7571–77580, 2002.

Open Access funding provided by 'Alma Mater Studiorum - Università di Bologna' within the CRUI CARE Agreement